

Local noncentrosymmetry and possible spin-momentum locking in $\text{Sr}_3\text{Ru}_2\text{O}_7$

Chenyi Shen,^{1,2,†} Hui Xing,^{3,†} Xinxin Cai,² David Fobes,⁴ Mingliang Tian,^{5,6}

Zhi-Qiang Mao,^{4,*} Zhuan Xu,^{1,6,*} and Ying Liu^{2,3,6,*}

¹Department of Physics, Zhejiang University, Hangzhou 310027, China

²Department of Physics and Materials Research Institute,

Pennsylvania State University, University Park, PA 16802, U.S.A.

³Key Laboratory of Artificial Structures and Quantum Control (Ministry of Education),
Department of Physics and Astronomy, Shanghai Jiao Tong University,
Shanghai 200240, China.

⁴Department of Physics, Tulane University, New Orleans, LA 70118, U.S.A.

⁵High Magnetic Field Laboratory, Chinese Academy of Science, Hefei 230031, China

⁶Collaborative Innovation Center of Advanced Microstructures, Nanjing 210093, China

†These authors contributed equally

*To whom correspondence should be addressed; E-mail:

mao@tulane.edu (Z-Q.M.) , zhuan@zju.edu.cn (Z.X.), and yxl15@psu.edu (Y.L.)

Strong spin-orbital coupling (SOC) was found previously to lead to dramatic effects in quantum materials, such as those found in topological insulators. It was shown theoretically that local noncentrosymmetry resulting from the rotation of RuO_6 octahedral in $\text{Sr}_3\text{Ru}_2\text{O}_7$ will also give rise to an effective SOC^{1,2}. In the presence of a magnetic field applied along a specific in-plane direction, the Fermi surface was predicted to undergo a reconstruction. Here we report results of our in-plane magnetoresistivity and magnetothermopower measurements on single crystals of $\text{Sr}_3\text{Ru}_2\text{O}_7$ with an electrical or a thermal current applied along specific crystalline directions and a magnetic field rotating in the ab plane (Fig. 1a), showing a minimal value for field directions predicted by the local noncentrosymmetry theory. Furthermore, the thermopower, and therefore, the electron entropy, were found to

be suppressed as the field was applied perpendicular to the thermal current, which suggests that the spin and the momentum in $\text{Sr}_3\text{Ru}_2\text{O}_7$ are locked over substantial parts of the Fermi surface, likely originating from local noncentrosymmetry as well.

Strontium ruthenates in the Roddlesden-Popper (R-P) series of $\text{Sr}_{n+1}\text{Ru}_n\text{O}_{3n+1}$ with a layered perovskite structure³ have attracted much attention since the discovery of superconductivity in the single-layer ($n = 1$) member of the series, Sr_2RuO_4 ⁴ and the subsequent demonstration of spin-triplet pairing in this material⁵. Work on other members of the series was motivated originally by the idea that the study of these materials would provide insight into the mechanism of spin-triplet superconductivity in Sr_2RuO_4 . Interestingly, these other members were found to feature novel phenomena themselves. In particular, the bilayer member, $\text{Sr}_3\text{Ru}_2\text{O}_7$, was found to be characterized by an anisotropic first-order metamagnetic transition⁶. When the field is along the c axis, the metamagnetic transition was found below ~ 1 K around 8 T. The end point of the first-order phase transition line was found around 100 mK^{7,8}, leading to the presence of a quantum critical end point (QCEP)^{6,9}. Near the QCEP, when the field was tilted slightly away from the c axis, the resistivity obtained with the measurement current perpendicular to the direction of the tilt is dramatically different from that obtained with the current parallel with the tilt in a narrow field range, a finding attributed to the emergence of a nematic phase¹⁰, Nematic Phase I, which was tied to the presence of the QCEP. For the in-plane field, the metamagnetic transition was found below ~ 1.2 K around 5 T, very different from those found for the c -axis field. A QCEP was found to be present only under a hydrostatic pressure^{11,12}. A large difference between values of resistivity obtained with the in-plane field applied parallel with and perpendicular to the measurement current was again found, but over a very large field range, and unrelated to the presence of QCEP. Even though this anisotropy was again linked to the presence of a nematic phase^{10,13}, Nematic Phase II, this phase must be very different from the

Nematic Phase I because the four-fold symmetry is already broken by the presence of the field. As a result, an anisotropy is expected to begin with.

The effect of the field orientation on metamagnetism in $\text{Sr}_3\text{Ru}_2\text{O}_7$ was attributed theoretically to a staggered SOC induced by local noncentrosymmetry, the breaking of local inversion symmetry due to the rotation of the RuO_6 octahedra about the c axis for about 6.8 degrees in $\text{Sr}_3\text{Ru}_2\text{O}_7$, which separates Ru sites into A and B sublattices¹. This doubles the unit cell in real space, or halves the first Brillouin zone in the momentum or k -space. Furthermore, the local noncentrosymmetry also enables the hopping between the p_x and the p_y orbitals of O ions that would have been forbidden in an undistorted tetragonal crystal. This SOC facilitates the coupling of t_{2g} orbitals of neighboring Ru ions which results in important features in the Fermi surface (FS) of $\text{Sr}_3\text{Ru}_2\text{O}_7$. Interestingly, this effect can be described by Rashba-like spin-orbit coupling (SOC), $\lambda L_z S_z$, where λ is the SOC strength, L_z the z -axis orbital angular momentum, and S_z the z component of the total spin^{1,2}. This picture explains the orientation dependence of metamagnetism in $\text{Sr}_3\text{Ru}_2\text{O}_7$. Under a magnetic field applied along the c axis, both L_z and S_z remain good quantum numbers. As a result, the effect of the SOC would be limited to the modification of the parameters in the Hamiltonian but not form of the Hamiltonian. Under the application of an in-plane field, however, staggered magnetic moments are induced on the A and B sublattices featuring an opposite canting angle with respect to the field direction, resulting in a net moment along the field direction and zero moment perpendicular to the field¹.

In the presence of an in-plane field, the local noncentrosymmetry in $\text{Sr}_3\text{Ru}_2\text{O}_7$ will also lead to the reconstruction of the FS through Pomeranchuk-type of effect, leading to corresponding change in the properties of the material^{1,2}. As shown in Fig. 1b, the FS of $\text{Sr}_3\text{Ru}_2\text{O}_7$ calculated in the tight-binding approximation and measured by angle resolved photo emission spectroscopy (ARPES) measurements¹⁴ features six bands: one electron- (the δ) and two hole-like (the α_1 and α_2) bands centered at the Γ point, other two electron-like (the β and γ_1) bands

around the M point, and finally, a very small hole-like (γ_2) band near the X point. Among these bands, the γ_2 pockets were found to be extremely close to a van Hove singularity¹⁴. Under a sufficiently strong in-plane field applied along the $\Gamma - X$ direction, the two γ_2 pockets of the FS in the direction of the field were predicted to be gapped out while each of the other two γ_2 pockets in the direction perpendicular to the field splits into two. Therefore, within this picture, the sample resistivity and thermopower, which are dependent on the scattering rate and the entropy of the charge carriers, respectively, would be expected to reach a minimum as the in-plane field is rotated to the $\Gamma - X$ direction.

We explored in the present work the effect of local noncentrosymmetry by performing magnetoresistivity and magnetothermopower measurements above the metamagnetic transition temperature on single crystals of $\text{Sr}_3\text{Ru}_2\text{O}_7$ cut along two separate crystalline directions with the field rotating in the ab plane. Specifically, a crystal of $\text{Sr}_3\text{Ru}_2\text{O}_7$ was cut along the a (or b) axis ([100] direction) or 45° away from them ([110] direction), resulting in a 90° - (the same as 0°) or 45° -cut crystal with a rectangular shape and measured by a steady-state technique (Fig. 1a) to ensure that the applied electrical or thermal current is along the desired direction in real and momentum (k) spaces. The direction of $-\nabla T$ relative to directions in the first Brillouin zone is shown schematically by the arrows in Fig. 1b for the 45° - and 90° -cut crystals. It is known that charge carriers on different parts of the FS contribute to resistivity and thermopower differently, reflected by a cosine of the angle between the \vec{k} vector and the electric or thermal current, $\theta_{\vec{k}}$ (Supplementary Information 1). For a 45° -cut crystal, the electric or thermal current is along $\Gamma - M$ direction, parts of the δ , $\alpha_{1,2}$, γ_1 and β sheets of the FS are perpendicular to (and the \vec{k} vector parallel with) the electric or thermal current, making the cosine factor maximal (~ 1); for a 90° -cut crystal, however, the electric or thermal current is along $\Gamma - X$ direction with parts of the δ , $\alpha_{1,2}$, and γ_2 sheets being perpendicular to the electric or thermal current. Therefore the 45° and 90° -cut crystals enable measurements on anisotropic transport properties arising from

anisotropic FS: those FS parts perpendicular to the applied electrical current or temperature gradient contribute the most to the sample resistivity or thermopower.

In Figs. 1c and d, thermopower, S , measured in c -axis oriented magnetic fields ($\mu_0 H_{\perp}$) of zero and 9 T, is plotted against the temperature, T . From 50 to 300 K, $S(T)$ of the 45° -cut crystal was found to vary linearly with temperature, dropping notably as the temperature fell below 50 K (Fig. 1c). In the 90° -cut crystal, the linear behavior is not seen. Instead, $S(T)$ was found to vary slowly for $T > 50$ K, dropping quickly again as the temperature fell below 50 K (Fig. 1d). In both crystals, $S(T)$ was found to show an increasing rate of decreasing as the temperature was lowered passing 17 K. The linear behavior in $S(T)$ is observed in most metals and attributed to the diffusion of free carriers¹⁵. The behavior seen in the 90° -cut crystal is clearly unconventional. Moreover, $S(T)$ is seen to be suppressed by the application of c -axis field of 9 T below 50 K, which signals the magnetic fluctuation contribution to the thermopower. In Figs. 1e and f, the Nernst signal, e_y , taken on crystals of both cuts with a 6 T magnetic field applied along the c axis, is plotted as a function of temperature. Above 50 K, the Nernst signal was found to be very small. The magnitude of Nernst coefficient e_y is seen to increase, reaching a maximum around 10 K, a temperature that is only slightly lower than the temperature at which a change of slope was seen in $S(T)$. It is interesting to note that at 17 K, a peak was seen in the temperature dependent magnetic susceptibility¹⁶ and Hall coefficients¹⁷ for $\text{Sr}_3\text{Ru}_2\text{O}_7$, attributed to the suppression of ferromagnetic fluctuation revealed by the inelastic neutron scattering (INS) measurements^{18,19}.

The systematic behavior seen in the thermopower and Nernst effect measurements is striking. According to the Heikes formula^{20,21},

$$S = \frac{\mu}{eT} = -\frac{\sigma}{e} \quad (1)$$

where μ is the chemical potential and σ is the entropy per electron, respectively. Therefore the thermopower measures the entropy of charge carriers on the FS. Furthermore, according to

the Mott formula^{22,23}, the sign of S for a particular band is determined mainly by the slope of $A(E)$ where A is the FS area. The ARPES studies showed that the FS sheets from the $\alpha_{1,2}$ and γ_2 bands are hole-like, leading to a positive contribution to S whereas Fermi surface sheets from the δ , β and γ_1 bands are electron-like, resulting in a negative contribution to S . Given that a positive rather than negative total S was obtained for $\text{Sr}_3\text{Ru}_2\text{O}_7$ at all temperatures, contribution from holes on the $\alpha_{1,2}$ and γ_2 sheets of FS should dominate the thermopower.

Measurements on the dependence of magnetothermopower on the angle between the in-plane magnetic field H_{\parallel} and $-\nabla T$, $S(\theta)$, where $\theta = 0^\circ$ corresponds to the case that the in-plane magnetic field is parallel with $-\nabla T$, were carried out. $S(\theta)$ taken on crystals of both cuts with an in-plane field of $\mu_0 H_{\parallel} = 6$ and 9 T showed that $S(\theta)$ possesses a four-fold symmetry, which is required by the crystalline symmetry. A significant observation, however, is that the minimal values in the thermopower were found when the in-plane field was aligned along the $\Gamma - X$ direction, as shown in Figs. 2a-d. Within the local noncentrosymmetry SOC picture, two γ_2 pockets along the field direction were gapped out so they no longer contribute to the thermopower, which will reduce the thermopower significantly despite of the small size of the γ_2 pockets because of the large density of states resulting from the proximity to a van Hove singularity. The other two γ_2 sheets that split into two under a high in-plane field will not contribute to thermopower at this field orientation for the 90° -cut crystal because the \vec{k} vectors of these pockets are essentially perpendicular to the direction of the thermal current at $\theta = 0^\circ$. For the 45° -cut crystal, the entropy from the surviving γ_2 pockets should be small because of the band splitting. The SOC originating from the local noncentrosymmetry should also have observable effect on the magnetoresistivity. Indeed, the normalized resistivity, $\rho/\bar{\rho}_{max}$ shown in Figs. 3a-d revealed a four-fold symmetry, again as demanded by the crystalline symmetry, and clear minimal value as the in-plane magnetic field is aligned along the $\Gamma - X$ direction, supporting the prediction that two γ_2 pockets are indeed gapped out in this case, as expected

in the local noncentrosymmetry picture.

In addition to a four-fold symmetry and minimal values in the $\Gamma - X$ direction, a strong two-fold anisotropy was also observed in $S(\theta)$. As seen in Fig. 2, at $T = 17$ K, the thermopower is suppressed when the in-plane field is perpendicular to $-\nabla T$ for the 45° -cut crystal for $\mu_0 H_{\parallel} = 6$ and 9 T, while for the 90° -cut crystal, the opposite was found under the same condition. Similarly, two-fold anisotropy was observed at $T = 20$ K and several higher temperatures (Figs. 4a and b). Because of the presence of an in-plane field, the two-fold anisotropy is also expected. Note that the in-plane fields used here, $\mu_0 H_{\parallel} = 6$ and 9 T, would have placed the system in the in-plane metamagnetic phase as the critical field of the transition is around 5 T. However, the temperatures at which the measurements were carried out were all higher than the critical temperature of the in-plane metamagnetic phase, ~ 1.2 K. At the lowest measurement temperature, 2 K, even though the two-fold anisotropy in $S(\theta)$ remains unchanged at 6 T, a dramatic change was found as the in-plane field was raised to 9 T. For crystals of both cuts, a two-fold anisotropy featuring a strong suppression of thermopower by an in-plane field applied perpendicular to $-\nabla T$ was found. The anisotropy change for the 90° -cut crystal featuring a 180-degree flip is particularly striking. Similarly, a two-fold anisotropy component is also seen in the normalized magnetoresistance, $\rho/\bar{\rho}_{max}$, but less anisotropic than that seen in the thermopower, and only in the 90° -cut crystal, as shown in Figs. 3a-d.

The above observation can be understood in the following scenario. Given that the two γ_2 pockets in the direction of the field are gapped out, and the other two γ_2 pockets do not contribute to thermopower or magnetoresistivity, as described above, a two-fold anisotropy in $S(\theta)$ on crystals of both cuts, and the same in $\rho(\theta)$ on the 90° -cut crystal, suggest that the entropy of charge carriers, possibly the scattering rate as well, is reduced when a sufficiently strong in-plane field is applied perpendicularly to the momenta of the charge carriers on the FS, which in turn suggests that spins are locked perpendicularly to their momenta on substantial

parts of the $\alpha_{1,2}$ sheets of FS. The application of an in-plane field along the direction of the locked spins would then tend to polarize the spin and reduce the entropy. Whether spins on the γ_2 pockets are locked to the momenta is not clear as the contribution of the surviving γ_2 pockets to the thermopower is minimal because of the cosine(θ) factor mentioned above. The absence of the two-fold anisotropy in $\rho(\theta)$ for the 45° -cut crystal is understandable as the magnetoresistivity reflects the scattering of charge carriers as well as the density of states, only the latter of which is tied directly to the entropy of a charge carrier.

The spin-momentum locking for carriers on the $\alpha_{1,2}$ sheets of the FS was not predicted in the local noncentrosymmetry SOC picture. In fact, the staggered magnetic moments induced by an in-plane magnetic field in the real space as predicted in this picture would imply that spins should be aligned along the applied field direction over the entire FS in high in-plane magnetic fields. However, in the zero or low in-plane field, spins on various sheets of the FS have their preferred direction because of the local noncentrosymmetry and orbital ordering as shown in the most recent theory of odd-parity electric octupole order featuring local electric quadrupoles arising from the Pomeranchuk instability and/or the orbital order alternatively stacked in the bilayers²⁴. In addition, the SOC from conventional sources, such as those found in Sr_2RuO_4 ²⁵, will also be present. It is entirely possible that spins on certain parts of the $\alpha_{1,2}$ sheets of the FS would prefer to align perpendicularly to momenta.

An interesting question is whether the effect of local noncentrosymmetry is temperature and (in-plane) field dependent. The line plots of the angle dependent normalized thermopower obtained on both 45° - and 90° -cut crystals at various temperatures are presented in Fig. 4a and 4b. Clearly the effect of the in-plane field on the thermopower as a function of temperature does not show a dramatic change as the temperature was passing through 17 K. Similarly, no dramatic changes are seen as the system entered the metamagnetic state (Figs. 4c and d). These observations suggest that spin-momentum locking in this material is insensitive to the

temperature and the field, consistent with the local noncentrosymmetry picture.

The spin-momentum locking and the nematicity found in $\text{Sr}_3\text{Ru}_2\text{O}_7$ ^{10,13} may be related. Evidently the c -axis nematic phase discovered originally is likely related to global physics such as Pomeranchuk type of Fermi surface instability near QCEP. In contrast, the in-plane-field nematicity, which seems to be less unexpected as the four-fold symmetry is already broken by the presence of the in-plane field, may be linked to local properties of the system such as the local noncentrosymmetry and resulted SOC. Finally, it is interesting to ask whether this effective SOC will lead to a topological phase. More theoretical studies are needed to understand our unexpected finding of the possible spin-momentum locking in $\text{Sr}_3\text{Ru}_2\text{O}_7$.

Methods

Single crystals of $\text{Sr}_3\text{Ru}_2\text{O}_7$ were grown by the floating zone method, as reported previously²⁶, and characterized by the x-ray diffraction, magnetization, and electrical transport measurements to ensure their quality (Supplementary Information 2). No secondary phases were detected in these screening measurements. Magnetoresistivity and thermoelectric measurements were carried out in a Quantum Design PPMS-9 system (featuring a base temperature of 1.8 K) using a steady-state technique. In this setup, a thermal gradient, $-\nabla T$, applied along the cut direction, 45° or 90° with respect to the a or b axis. The temperature gradient was determined by a pair of differential type E thermocouples, and was set to around 0.5 K/mm.

References

1. Fischer, M. H. & Sigrist, M. Effect of a staggered spin-orbit coupling on the occurrence of a nematic phase in $\text{Sr}_3\text{Ru}_2\text{O}_7$. *Phys. Rev. B* **81**, 064435 (2010).
2. Puetter, C. M., Rau, J. G. & Kee, H.-Y. Microscopic route to nematicity in $\text{Sr}_3\text{Ru}_2\text{O}_7$. *Phys. Rev. B* **81**, 081105 (2010).

3. Ruddlesden, S. N. & Popper, P. The compound $\text{Sr}_3\text{Ti}_2\text{O}_7$ and its structure. *Acta Crystallogr.* **11**, 54–55 (1958).
4. Maeno, Y. *et al.* Superconductivity in a layered perovskite without copper. *Nature* **372**, 532–534 (1994).
5. Mackenzie, A. P. & Maeno, Y. The superconductivity of Sr_2RuO_4 and the physics of spin-triplet pairing. *Rev. Mod. Phys.* **75**, 657–712 (2003).
6. Perry, R. S. *et al.* Metamagnetism and critical fluctuations in high quality single crystals of the bilayer ruthenate $\text{Sr}_3\text{Ru}_2\text{O}_7$. *Phys. Rev. Lett.* **86**, 2661–2664 (2001).
7. Grigera, S. A. *et al.* Magnetic field-tuned quantum criticality in the metallic ruthenate $\text{Sr}_3\text{Ru}_2\text{O}_7$. *Science* **294**, 329–332 (2001).
8. Rost, A. W. *et al.* Thermodynamics of phase formation in the quantum critical metal $\text{Sr}_3\text{Ru}_2\text{O}_7$. *Proc. Nat. Acad. Sci.* **108**, 16549–16553 (2011).
9. Ohmichi, E. *et al.* Double metamagnetic transition in the bilayer ruthenate $\text{Sr}_3\text{Ru}_2\text{O}_7$. *Phys. Rev. B* **67**, 024432 (2003).
10. Borzi, R. A. *et al.* Formation of a nematic fluid at high fields in $\text{Sr}_3\text{Ru}_2\text{O}_7$. *Science* **315**, 214–217 (2007).
11. Wu, W. *et al.* Quantum critical metamagnetism of $\text{Sr}_3\text{Ru}_2\text{O}_7$ under hydrostatic pressure. *Phys. Rev. B* **83**, 045106 (2011).
12. Sun, D. *et al.* Pressure study of nematicity and quantum criticality in $\text{Sr}_3\text{Ru}_2\text{O}_7$ for an in-plane field. *Phys. Rev. B* **88**, 235129 (2013).
13. Mackenzie, A. P., Bruin, J. A. N., Borzi, R. A., Rost, A. W. & Grigera, S. A. Quantum

- criticality and the formation of a putative electronic liquid crystal in $\text{Sr}_3\text{Ru}_2\text{O}_7$. *Physica C: Superconductivity* **481**, 207 – 214 (2012).
14. Tamai, A. *et al.* Fermi surface and van hove singularities in the itinerant metamagnet $\text{Sr}_3\text{Ru}_2\text{O}_7$. *Phys. Rev. Lett.* **101**, 026407 (2008).
 15. Cusack, N. & Kendall, P. The absolute scale of thermoelectric power at high temperature. *Proc. Phys. Soc.* **72**, 898 (1958).
 16. Ikeda, S.-I., Maeno, Y., Nakatsuji, S., Kosaka, M. & Uwatoko, Y. Ground state in $\text{Sr}_3\text{Ru}_2\text{O}_7$: fermi liquid close to a ferromagnetic instability. *Phys. Rev. B* **62**, R6089–R6092 (2000).
 17. Liu, Y. *et al.* Electrical transport properties of single-crystal $\text{Sr}_3\text{Ru}_2\text{O}_7$: The possible existence of an antiferromagnetic instability at low temperatures. *Phys. Rev. B* **63**, 174435 (2001).
 18. Capogna, L. *et al.* Observation of two-dimensional spin fluctuations in the bilayer ruthenate $\text{Sr}_3\text{Ru}_2\text{O}_7$ by inelastic neutron scattering. *Phys. Rev. B* **67**, 012504 (2003).
 19. Ramos, S. *et al.* Spin dynamics in near the metamagnetic transition by inelastic neutron scattering. *Physica B: Condensed Matter* **403**, 1270 – 1272 (2008).
 20. Chaikin, P. M. & Beni, G. Thermopower in the correlated hopping regime. *Phys. Rev. B* **13**, 647–651 (1976).
 21. Beni, G. Thermoelectric power of the narrow-band hubbard chain at arbitrary electron density: Atomic limit. *Phys. Rev. B* **10**, 2186–2189 (1974).
 22. Blatt, F. J., Schroeder, P. A., Foiles, C. L. & Greig, D. *Thermoelectric power of metals* (Plenum Press, New York, 1976).
 23. Barnard, R. *Thermoelectricity in metals and alloys* (Halsted Press, New York,1972).

24. Hitomi, T. & Yanase, Y. Electric octupole order in bilayer ruthenate $\text{Sr}_3\text{Ru}_2\text{O}_7$. *J. Phys. Soc. Jpn.* **83**, 114704 (2014).
25. Haverkort, M. W., Elfimov, I. S., Tjeng, L. H., Sawatzky, G. A. & Damascelli, A. Strong spin-orbit coupling effects on the fermi surface of Sr_2RuO_4 and Sr_2RhO_4 . *Phys. Rev. Lett.* **101**, 026406 (2008).
26. Ikeda, S. I., Azuma, U., Shirakawa, N., Nishihara, Y. & Maeno, Y. Bulk single-crystal growth of strontium ruthenates by a floating-zone method. *J. Cryst. Growth* **237**, **39**, Part **1**, 787 - 791 (2002).

Acknowledgements

The authors have benefited from discussions with Hae-Young Kee and Yayu Wang. The work done at Penn State is supported by DOE under DE-FG02-04ER46159, at SJTU by MOST of China (2012CB927403) and NSFC (11274229, 11474198 and 11204175), at ZJU by MOST of China (2012CB927403) and NSFC (U1332209), at CAS by NSFC (U1432251), and at Tulane by NSF under DMR-1205469.

Author contributions

C.S. and H.X. prepared the sample, performed the measurements, analyzed the data, and wrote the manuscript. X.C. perform the measurements and analyzed the data. D.F. grew the crystals. M.T. performed measurements. Z-Q.M. and Z.X. analyzed the data and wrote the manuscript. Y.L. designed experiment, analyzed the data, and wrote the manuscript.

Competing financial interests

The authors declare no competing financial interests.

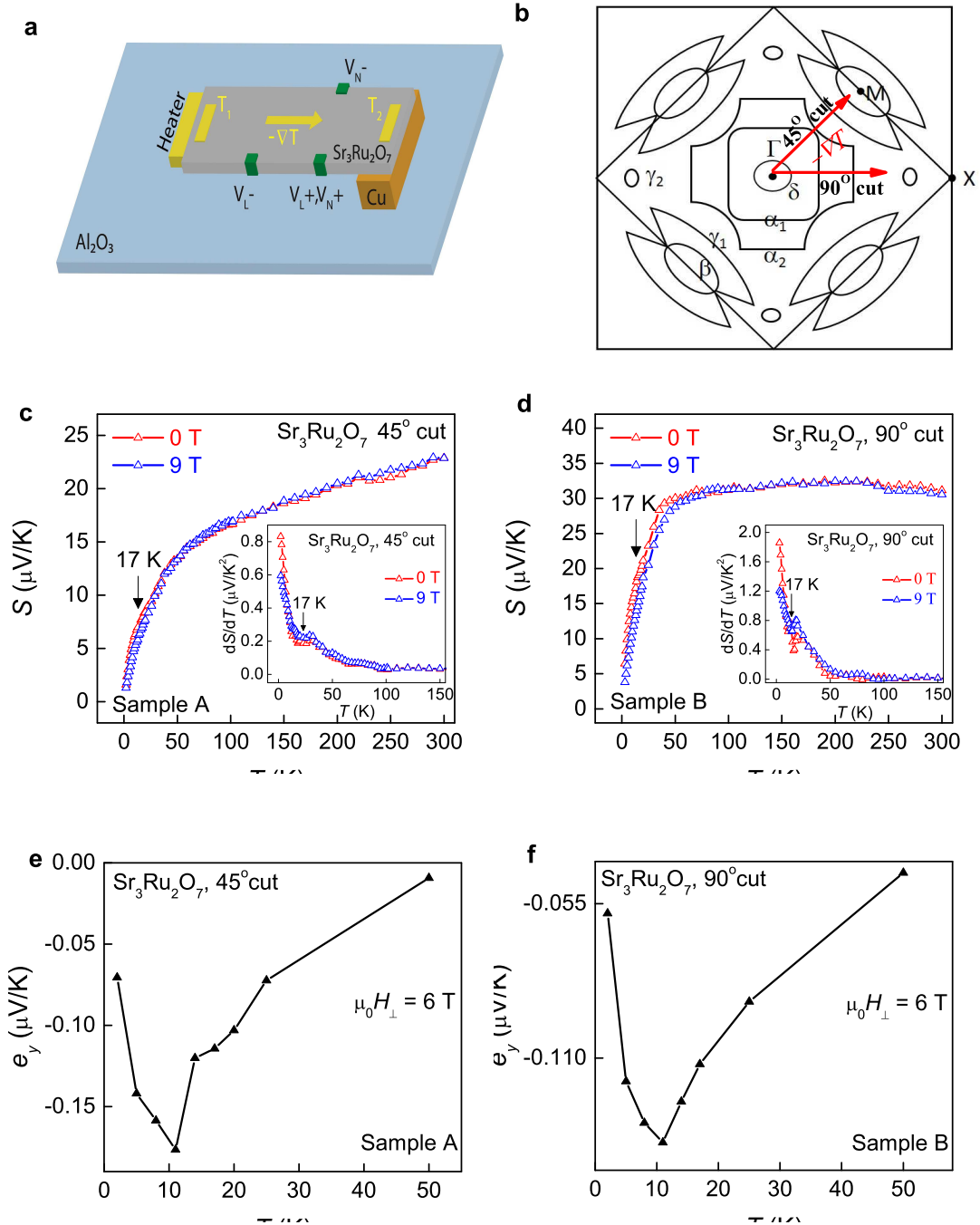


Figure 1 | Experimental schematics and thermoelectric properties with magnetic field along c

axis. **a**, The sample configuration for magnetothermoelectric measurements. **b**, Schematics showing the direction of $-\nabla T$ relative to directions in the first Brillouin zone for a 45° - and 90° -cut crystal, respectively. Here $\Gamma - X$ is along the direction of Ru-O-Ru in real space; **c**, **d**, Thermopower, S as a function of temperature (T) with a magnetic field (H) applied along the c axis for a 45° - and 90° -cut crystal, respectively. Inset: dS/dT plotted against T , with a feature seen at 17 K; **e**, **f**, The Nernst signal, e_y as a function of T with a field, $\mu_0 H_\perp = 6$ T, applied along the c axis for a 45° - and 90° -cut crystal, respectively.

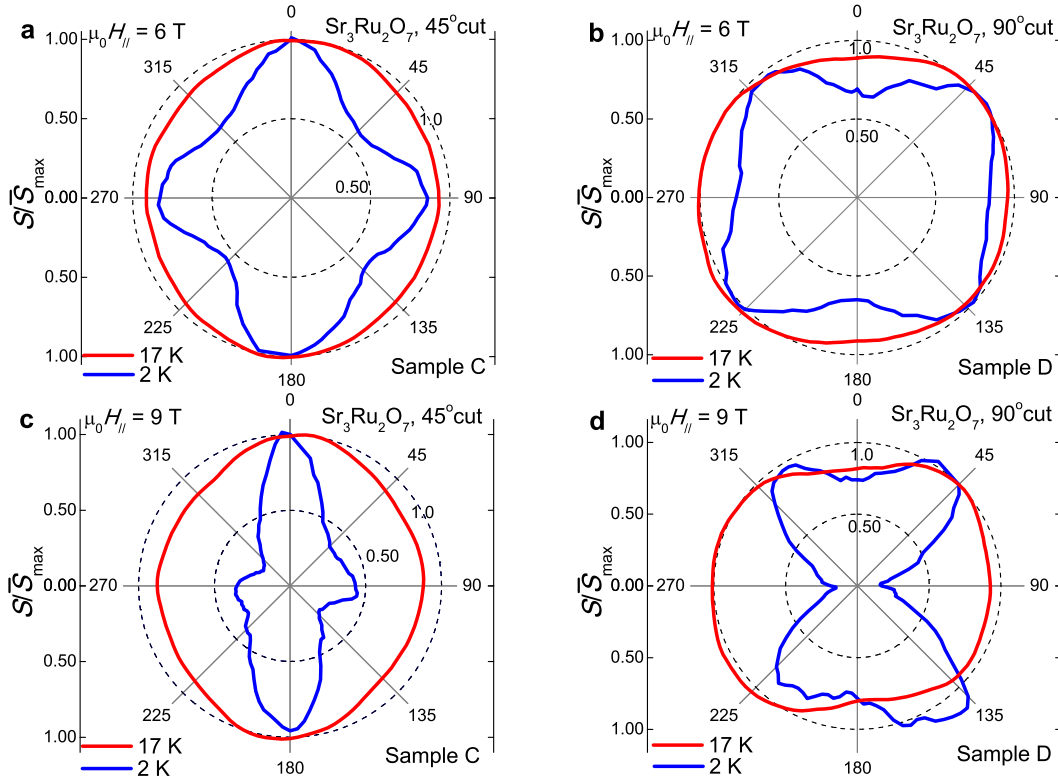


Figure 2 | Normalized thermopower S/\bar{S}_{max} as a function of the rotating angle of the in-plane field. **a**, **c** are for the 45° -cut crystal; **b**, **d** are for the 90° -cut crystal. Here \bar{S}_{max} is the average of four maximal S values and $\theta = 0^\circ$ corresponds to the direction for which the magnetic field is parallel with $-\nabla T$, which is $\Gamma - M$ for the 45° - and $\Gamma - X$ for the 90° -cut crystal, respectively. The four-fold symmetry is expected from the crystalline symmetry. The two-fold anisotropy is also

seen under certain conditions as noted. A minimum was observed in all cases when the in-plane field is placed along the $\Gamma - X$ direction.

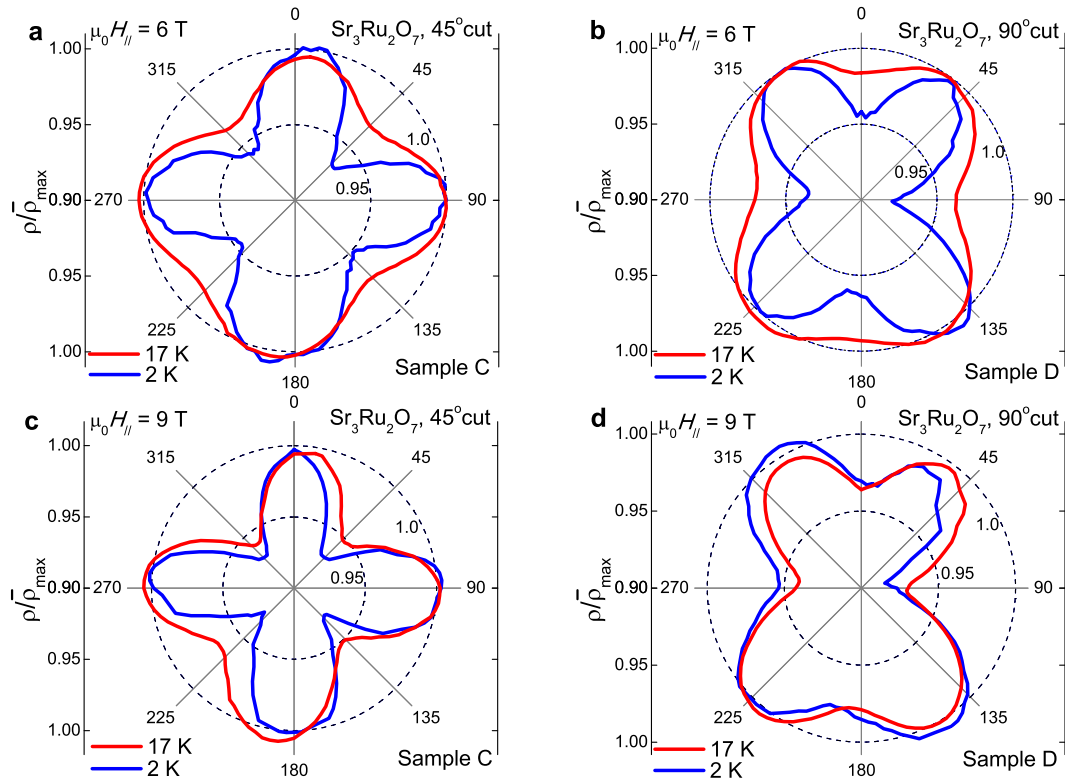


Figure 3 | Normalized resistivity $\rho/\bar{\rho}_{max}$ as a function of the rotating angle of the in-plane field. a, c are for the 45° -cut crystal; b, d are for the 90° -cut crystal. Two-fold anisotropy is also seen in $\rho/\bar{\rho}_{max}$ for the 90° -cut (b, d) crystal, but less dramatic than that seen in $S(\theta)$.

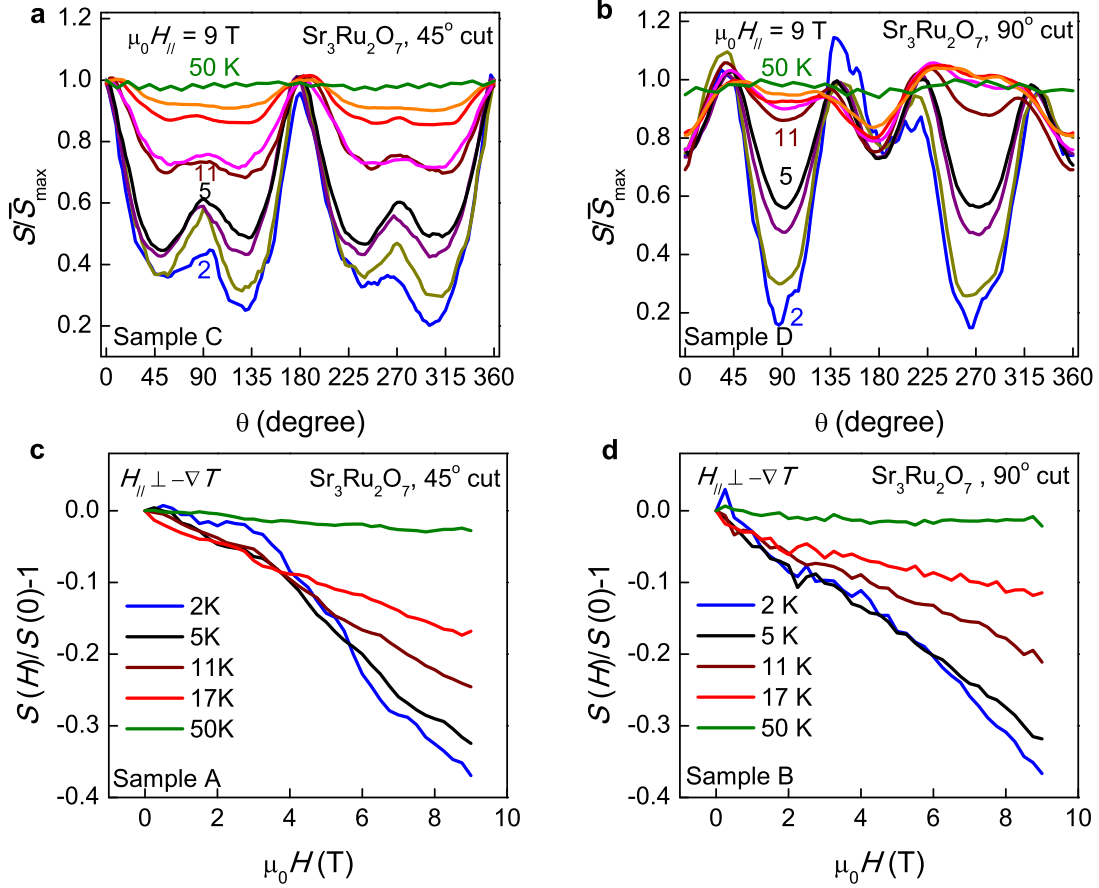


Figure 4 | Temperature and field evolution of normalized thermopower. **a, b,** Temperature evolution of normalized thermopower S/\bar{S}_{\max} as a function of the rotating angle of a 9 T in-plane field for a 45°- and 90°-cut crystal, respectively. From bottom to top $T = 2, 3, 4, 5, 11, 14, 17, 20$ and 50 K. No abrupt change is seen in the anisotropy as the temperature is lowered; **c, d,** The normalized thermopower, $S(H)/S(0) - 1$, as a function of the in-plane magnetic field applied nearly perpendicularly to thermal gradient (within a few degrees) at fixed temperatures for a 45°- and 90°-cut single crystal, respectively.